ELSEVIER

Journal of Molecular Catalysis A: Chemical 169 (2001) 275–287

JOURNAL OF MOLECULAR CATALYSIS A: CHEMICAL

www.elsevier.com/locate/molcata

Effects of Al/Zr ratio on ethylene–propylene copolymerization with supported-zirconocene catalysts

Mônica Carcuchinski Haag [a], Cristiano Krug [a], Jairton Dupont [a], Griselda Barrera de Galland [a], João Henrique Zimnoch dos Santos [a,*], Toshiya Uozumi [b], Tsuneji Sano [b], Kazuo Soga [b,†]

[a] *Instituto de Química, Universidade Federal do Rio Grande do Sul, Av. Bento Gonçalves, 9500-91509-900 Porto Alegre RS, Brazil*
[b] *School of Materials Science, Japan Advanced Institute of Science and Technology, 1-1 Asahidai, Tatsunokuchi, Ishikawa 923-1292, Japan*

Received 16 October 2000; received in revised form 4 January 2001; accepted 4 January 2001

Abstract

Effects of heterogenization parameters on compositional and catalytic properties of $Et(Ind)_2ZrCl_2$ supported on silica modified with MAO were evaluated using data on metal loading, catalyst activity in ethylene–propylene copolymerization, and polymer properties. The supported catalysts were prepared according to a 2^3 factorial design for multivariate analysis. The parameters studied were: MAO concentration in impregnation, $Et(Ind)_2ZrCl_2$ concentration in grafting, and immobilization temperature for both metallocene and organoaluminum. The grafting solution was monitored by UV–VIS spectroscopy, while the resulting catalyst systems were characterized by inductively-coupled plasma-optical emission spectroscopy (ICP-OES), diffuse reflectance infrared Fourier transform spectroscopy (DRIFTS), and X-ray photoelectron spectroscopy (XPS). At high statistical significance, both MAO and $Et(Ind)_2ZrCl_2$ concentrations during preparation affected the determination of the final Al/Zr ratio on silica. The catalyst systems were tested in ethylene–propylene copolymerizations using external MAO as cocatalyst. Relationships were observed between (i) catalyst activity and the binding energy of Zr $3d^{5/2}$ electrons and (ii) Al/Zr ratio on silica and the average ethylene incorporation. The polymer samples presented narrow molecular weight distribution, but according to differential scanning calorimetry (DSC), and cross-fractionation chromatography (CFC) data, catalyst systems with given Al/Zr ratios might yield different crystallites, suggesting a plural distribution of chemical composition.

Keywords: Ethylene–propylene copolymerization; Metallocene catalysts; Supported metallocene; XPS

1. Introduction

Metallocene catalysts have been widely studied in copolymerization reactions aiming at producing materials with improved properties [1]. They provide higher activity, narrower molecular weight distribution (MWD), and narrower chemical composition distribution (CCD) compared to conventional Ziegler–Natta catalysts [2,3]. Moreover, such catalyst systems lead to lower residual metal contents [4]. Nevertheless, their heterogenization is mandatory for commercial production using existing plants (*drop-in technology*). Metallocene immobilization protocols have been constantly reviewed in the literature [5–7].

Large-scale ethylene–propylene (EP) copolymer production is currently based on vanadium and

* Corresponding author. Fax: +55-51-319-1499.
E-mail address: jhzds@if.ufrgs.br (J.H.Z. dos Santos).
† Deceased.

1381-1169/01/$ – see front matter
PII: S1381-1169(01)00045-0

titanium catalysts in well-known Ziegler–Natta polymerization processes. Blending these high-flex modulus resins with PP converts them to rubbers forming the TPEs (thermoplastic elastomers). Such approach allows their use in the automotive industry, wire and cable coating, adhesives, and a variety of mechanical parts. The wide range of applications can be evaluated by the worldwide consumption of TPEs, which in 1998 was estimated as ca. 1.3×10^6 tonnes per year [8].

There are some comparative studies in the literature for soluble metallocene systems in the production of EP copolymers [9–12]. For instance, a comparison of bridged and non-bridged catalysts shows that the latter, such as $(n\text{BuCp})_2ZrCl_2$, lead to higher molecular weight but lower propylene incorporation [11,12]. The bridged systems can produce polymers with different monomer incorporation and consequently different physical properties. This flexibility makes them more attractive for commercial copolymer production. Many other systems have been proposed in the literature aiming at preventing low molecular weights at high comonomer incorporation [13–16].

Concerning supported zirconocenes, in a pioneer work, Chien and He [17] studied the influence of the Al/Zr ratio in the polymerization milieu on catalyst activity and on polymer properties using silica pretreated with MAO as support. Under their experimental conditions, the authors concluded that there was no effect on the nature of polymerization-active species, because metallocene immobilization on the support was mediated by MAO. Nevertheless, other studies indicate that catalyst heterogenization can change the polymerization mechanism (and consequently the polymer final properties), due to interactions between the metallocene catalyst and the support [18–20].

Following our previous works [21,22], we discuss in the present paper, the influence of heterogenization parameters on the nature of the supported-catalyst species and on EP copolymer properties for $Et(Ind)_2ZrCl_2/MAO/SiO_2$ systems. Experiments were performed according to a 2^3 factorial design, and the catalyst systems were characterized by inductively-coupled plasma-optical emission spectroscopy (ICP-OES), diffuse reflectance infrared Fourier transform spectroscopy (DRIFTS), and X-ray photoelectron spectroscopy (XPS). The resulting catalysts were tested in EP copolymerization, using external MAO as cocatalyst. The copolymers were characterized by gel permeation chromatography (GPC), ^{13}C nuclear magnetic resonance (^{13}C NMR), differential scanning calorimetry (DSC), and cross-fractionation chromatography (CFC).

2. Experimental

2.1. Chemicals

Polymerization grade ethylene (Copesul S.A., Triunfo, Brazil) and propylene (White Martins, Porto Alegre, Brazil) were dried through columns of 0.4 nm molecular sieve. Toluene (Nuclear, Porto Alegre, Brazil) was dried by refluxing over metallic sodium followed by distillation under argon atmosphere. The catalyst precursor $Et(Ind)_2ZrCl_2$ and the cocatalyst MAO (methylaluminoxane) were supplied by Witco (Mechelen, Belgium), while silica Davison 948 ($255\,m^2\,g^{-1}$) was purchased from Grace (Baltimore, USA). All the chemicals were manipulated in inert atmosphere using the Schlenk technique.

2.2. Catalyst preparation

The supported catalysts were prepared according to a 2^3 factorial design for multivariate analysis [23]. The studied variables were: immobilization temperature (303 or 353 K), MAO concentration in the impregnation solution (6 or 12 wt.% Al/SiO_2), and zirconocene concentration in the grafting solution (1.5 or 2.5 wt.% Zr/SiO_2) (see Table 1).

Silica was activated at 723 K for 18 h under vacuum ($<10^{-4}$ mbar) prior to chemical modification by impregnation with ca. 10 ml of a solution of MAO in toluene with Al concentration corresponding to the experimental plan. The MAO solution was added to 1.0 g of silica under dry argon, the slurry was magnetically stirred for 1 h at one of the studied temperatures, and the solvent was completely evaporated under reduced pressure. In a second step, ca. 10 ml of a solution of $Et(Ind)_2ZrCl_2$ in toluene with concentration corresponding to the desired Zr/SiO_2 ratio was added to the modified silica under dry argon, and the slurry was magnetically stirred for 1 h at the chosen immobilization temperature. The grafting procedure

Table 1
Catalyst preparation conditions and final metal loading

Preparation	Factor			Response		
	Temperature (K)	Zr/SiO_2 (wt.%)	Al/SiO_2 (wt.%)	Zr/SiO_2 (wt.%)	Al/SiO_2 (wt.%)	Zr $3d^{5/2}$ FWHM (eV)
1	353	2.5	12	1.2	7.8	2.0
2	353	2.5	6	1.8	6.6	2.6
3	353	1.5	12	0.7	13.0	2.3
4	353	1.5	6	1.2	5.8	2.4
5	303	2.5	12	0.8	6.7	2.0
6	303	2.5	6	1.7	2.2	2.8
7	303	1.5	12	0.8	9.3	2.1
8	303	1.5	6	1.0	7.1	2.5

[24] was concluded by filtering the slurry and washing the separated solid with 10 aliquots of 2 ml of toluene. The grafting solution was analyzed by means of ultraviolet/visible (UV–VIS) spectroscopy (Shimadzu, UV-1601pcs, Kyoto, Japan) in the 300–600 nm wavelength range using a quartz cell (1.0 cm path length) attached to a Schlenk flask, as described in the literature [25].

2.3. Catalyst characterization

Samples were submitted to acid digestion in a microwave system (CEM, MDS 2000, Matthews, USA). Al and Zr concentrations were measured by ICP-OES (Perkin-Elmer, Optima 3000, Norwalk, USA).

UV–VIS analysis was performed in a DW-2000 spectrometer (SLM-Aminco, Rochester, USA) equipped with a beam scrambler, which diffuses the entering light to form a uniform field of illumination. In order to increase the transparency of the samples and the viscosity of the milieu, the solids were mixed with Nujol to form a slurry. All the samples were prepared in a glove box in quartz cells (1.0 cm path length). The absorption spectra were recorded under dry N_2 between 250 and 550 nm having Nujol as reference.

The DRIFTS measurements were made on a BOMEM FT-IR spectrophotometer (MB-102, Que., Canada) at 298 K co-adding 32 scans at a resolution of 4 cm^{-1}. The measurements were restricted to the 4000–2600 cm^{-1} region. The samples were analyzed as powders in a DRIFT accessory equipped with sampling cups. The spectra were collected in reflectance units and transformed to Kubelka–Munk units.

The XPS were obtained on a PHI 5600 Esca System (Φ Physical Electronics, Eden Prairie, USA), using monochromated Al Kα radiation (1486.6 eV). Spectra were taken at room temperature in low resolution (pass energy 235 eV) in the binding energy range of 1000–0 eV and in high-resolution (pass energy 23.5 eV) modes for the Si 2p, Al 2p, and Zr $3d^{5/2}$ regions. The samples were mounted on an adhesive copper tape as thin films. They were prepared in a glove box and transferred under nitrogen atmosphere. Each sample was analyzed at a 75° angle between the sample surface and the axis of the photoelectron energy analyzer. All binding energies were charge-referenced to the silica Si 2p at 103.3 eV. More details of measurement conditions can be found elsewhere [26].

2.4. Polymerization reactions

Polymerizations were carried out in a 1 l glass reactor using toluene as solvent and ca. 50 mg of supported catalyst. The external MAO (0.006 mol Al) and the catalyst were introduced in this order into the reactor containing 0.3 l of toluene under continuous flow of a mixture of ethylene and propylene (60/40 in mass, controlled by mass flow controllers at 328 K). A detailed discussion about this polymerization procedure can be found elsewhere [27,28], in which experimental and theoretical studies for this semi-batch operation mode are reported. After 30 min, the reaction was quenched by the addition of ethanol. The polymer was collected, washed with ethanol, and vacuum dried at room temperature for 16 h.

2.5. Polymer characterization

^{13}C NMR spectroscopy was used to determine propylene incorporation and polymer microstructure. Chemical shifts were referenced internally to the major backbone methylene resonance (taken as 30.00 ppm from Me_4Si) and calculated according to the rules of Linderman and Adams [29]. Sample solutions were prepared in *o*-dichlorobenzene and benzene-d_6 (20 vol.%) in a sample tube of 5 mm diameter. The deuterated solvent was used to provide the internal lock signal. The ^{13}C NMR spectra were obtained at 353 K in an Inova 300 equipment (Varian Associates, Palo Alto, USA) operating at 75 MHz. Spectra were taken with a 70° flip angle, an acquisition time of 1.5 s, and a delay of 4.0 s.

The glass transition temperature (T_g) of the polymers was determined using differential scanning calorimetry (1200 PL-DSC, Polymer Laboratories, Church Stretton, UK). Heating and cooling cycles at the rate of 20 K min^{-1} in the temperature range 173–423 K were performed twice, but only the results from the second cycle are reported.

Molar masses and molar mass distributions were investigated with a high-temperature GPC instrument (Waters, 150CV Plus, Milford, USA) equipped with an optical differential refractometer and three Styragel HT type columns (HT3, HT4, and HT6) with exclusion limit 1×10^7 for polystyrene; 1,2,4-trichlorobenzene was used as solvent, at a flow rate of 1 cm^3 min^{-1} and the analyses were performed at 413 K. The columns were calibrated with standard narrow molar mass distribution polystyrenes and with standard polyethylene and polypropylenes.

CFC of polymer samples was carried out on a Mitsubishi Petrochemical CFC T-150 (Tokyo, Japan) with a flow rate of 1.0 cm^3 min^{-1}, using *o*-dichlorobenzene as solvent.

3. Results and discussion

3.1. Catalyst systems

In a previous work, we determined the adsorption isotherms of MAO and Cp_2ZrCl_2 on silica [24]. Some experimental parameters in the preparation of (nBuCp)$_2ZrCl_2$-supported catalysts were also studied; among them, the grafting temperature was shown to influence both the supported-metal loading and the catalyst activity [30]. Based on such previous results, we decided to perform a study of the influence of immobilization temperature and of initial MAO and metallocene concentrations in the case of grafting $Et(Ind)_2ZrCl_2$ on silica chemically modified with MAO. Application of the experimental design permits the optimization of a number of experiments and convenient access to the experimental uncertainties intrinsic to analytical data [23]. For each variable, two levels were adopted: 303 or 353 K for grafting temperature, 6 or 12 wt.% Al/SiO_2 for MAO concentration, and 1.5 or 2.5 wt.% Zr/SiO_2 for metallocene concentration. The values correspond to Al and Zr concentrations below and above the saturation loading on silica Davison 948 [29].

Table 1 shows catalyst system preparation conditions and the resulting metal loading on silica. Analysis of variance at the 95% confidence level indicates that only the original concentrations of zirconocene and MAO in solution are significant for immobilized Zr amount. Calculated effects [23] indicate that increasing Al concentration in the impregnation solution from 6 to 12 wt.% Al/SiO_2 reduces the final Zr loading on silica in average 0.54 wt.% Zr/SiO_2. On the other hand, increasing zirconocene concentration in the grafting solution from 1.5 to 2.5 wt.% Zr/SiO_2 increases the final Zr loading on silica in average 0.47 wt.% Zr/SiO_2.

Concerning the Al immobilized content, none of the studied factors (temperature and concentrations of MAO and zirconocene) showed statistical significance at the 95% confidence level; the final loading on silica is probably determined by the number of available immobilization sites (isolated silanol groups at the silica surface) and by leaching during the zirconocene grafting step, as seen by UV–VIS and XPS analyses and discussed ahead. Besides the isolated Zr and Al metal loading, a property that is generally useful in the description of zirconocene systems is the Al/Zr immobilized ratio. Once again considering the 95% confidence level, this ratio is significantly influenced by the MAO concentration in the impregnation solution. The change from 6 to 12 wt.% Al/SiO_2 in the preparation step increases in average the Al/Zr ratio fixed on the support. Later, the resulting chemical composition of the copolymers will be correlated to this parameter.

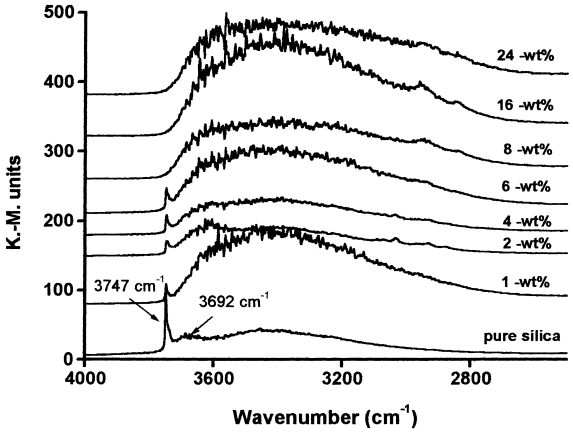

Fig. 1. DRIFTS spectra of MAO-modified silicas. Al contents from 0 to 24 wt.% Al/SiO_2.

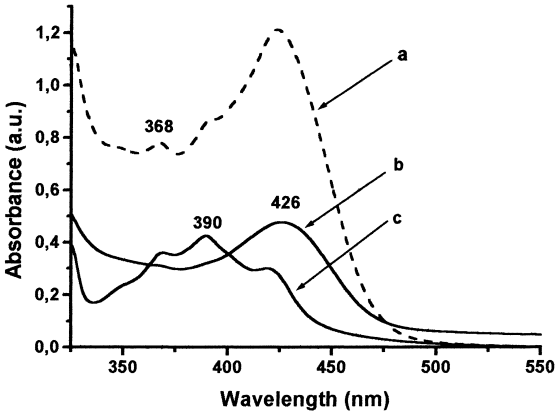

Fig. 2. UV–VIS spectra in toluene: (a) grafting solution, 12.0 wt.% Al/SiO_2; (b) $Et(Ind)_2ZrCl_2$, 2×10^{-4} mol l^{-1}; (c) grafting solution, 6.0 wt.% Al/SiO_2.

A better understanding of these results requires a deeper insight at the phenomena occurring on the silica surface by the action of MAO and the zirconocene. Fig. 1 shows DRIFTS spectra taken from thermally activated silica before and after the treatment with different amounts of MAO. The sharp peak at 3747 cm^{-1} has been assigned to isolated silanol groups, while the broad band centered at 3692 cm^{-1} to OH groups retained inside pores (intraglobular) [31]. It can be seen that at low MAO contents (1.0–6.0 wt.% Al/SiO_2), there is still a fraction of isolated silanol groups, which are totally consumed at higher MAO contents (8.0–24.0 wt.% Al/SiO_2), evidencing chemical saturation of the silica surface. This behavior is in accordance with our previous results concerning the MAO adsorption isotherm on silica Davison 948 under the same temperature pretreatment conditions [24]. Since, silanol groups are potential immobilization sites for both MAO and the metallocene, in silica initially treated with 6.0 wt.% Al/SiO_2, there are still isolated silanol groups on the surface for anchoring of the metallocene. In this case, zirconocene immobilization is expected to occur both on the remaining silanol groups and on the MAO coating. The mean molar ratio Al/(isolated OH) found for the eight preparations was 4.3, indicating that most Al atoms are not directly bonded to the support, but through the cage structure of MAO.

In the case of impregnation with 12 wt.% Al/SiO_2, part of the MAO is expected to remain only physisorbed on the coated support, since this concentration corresponds to a metal content above saturation. This fraction should then be at least partially removed during the grafting step, leading to soluble species that can be detected by UV–VIS analysis.

The UV–VIS spectrum of the grafting solution corresponding to 12 wt.% Al/SiO_2 (spectrum (a) in Fig. 2) shows three bands at 426, 390, and 368 nm. The band at 426 nm has been attributed to a ligand-to-metal charge transfer process (LMCT) in $Et(Ind)_2ZrCl_2$ (spectrum (b)) [32]. The band at 390 nm was observed for the system $Et(Ind)_2ZrCl_2$/MAO, $Al/Zr = 30$, and attributed to a methyl derivative of the precursor (monoalkylated species) [25]. The band centered at 368 nm is probably due to the dimethyl derivative of the original metallocene, as observed for other metallocene catalysts [33]. In the case of the grafting solution for 6 wt.% Al/SiO_2, only the band corresponding to the catalyst precursor (426 nm) is clearly observed. The concentration of the catalyst precursor in the grafting filtrate was estimated from the 426 nm band for the preparations using 12 and 6 wt.% Al/SiO_2 and was found to be 13.6 and 4.2 mol%, respectively. This result confirms the statistical analysis for the catalyst grafting, i.e. modification of silica with 12 wt.% Al/SiO_2 yields lower Zr loading compared to modification with 6 wt.% Al/SiO_2.

UV–VIS analysis of a supported catalyst is shown in Fig. 3. Three bands appear at 385, 364, and 297 nm. As discussed earlier, the bands at 364 and 385 nm can

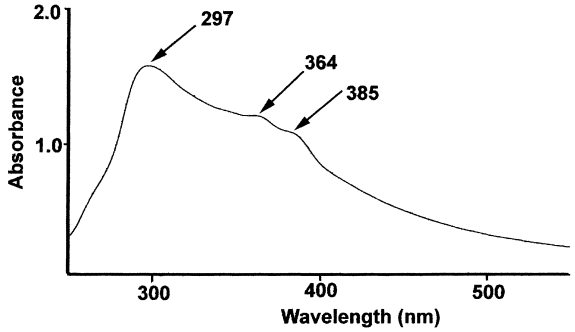

Fig. 3. UV–VIS spectrum of the supported catalyst (preparation 7).

be attributed to the mono- and dimethylated species, respectively. The band at 297 nm corresponds to MAO [32]. It is also important to note that the band relative to the catalyst precursor (426 nm) is absent. This indicates that alkylated species are generated on the silica surface upon immobilization of the catalyst precursor.

The XPS technique has been used to identify and quantify surface species, as well as to study the chemical environment of metal atoms in catalysts [34]. As analysis is restricted to the sample surface, the results obtained from this technique cannot be directly compared with those of bulk-sensitive techniques. An XPS survey scan was performed on the supported catalysts in view of elemental analysis. A representative survey spectrum is shown in Fig. 4. All constituent atoms of the catalysts (Si, O, Cl, Zr, Al, and C) were observed with in the XPS sampling depth (approximately 3 nm). When one of the peaks of a survey spectrum is examined under conditions of higher energy resolution, the position of the maximum is found to depend on the chemical environment of the atom responsible for the peak. Variations in the number of valence electrons and types of bonds they form influence the binding energies of core electrons. Binding energies increase as the oxidation state becomes more positive. XP spectra provide not only qualitative information about types of atoms present in a compound but also the relative number of each type. Insulating samples (as in the present case) are prone to charging effects, which can be overcome by means of an electron gun during the measurement.

XPS core level spectra of Si, Al, and Zr were recorded in high resolution mode. The Si 2p spectrum presents two signals: 103.3 and 101.7 eV, attributable, respectively, to Si atoms in the bulk and at the external surface (Fig. 5a). For Al, XPS analyses show the presence of two signals that denote Al atoms in different chemical environments: ca. 72.0 and 74.0 eV (Fig. 5b). The latter, whose binding energy (BE) is typical of Al–O moieties, corresponds to ca. 90% of the total area. The former suggests Al atoms in environment rich in electron density, related probably to anionic species generated on the surface.

Fig. 5c shows the Zr 3d spectrum of a supported system. The presence of two signals is due to spin–orbit coupling of the 3d electrons of Zr: ca. 183 eV ($3d^{5/2}$) and 185 eV ($3d^{3/2}$). Deconvolution of the spectra suggests the presence of two species.

Analysis of the full width at half maximum (FWHM) intensity of the Zr $3d^{5/2}$ peaks (considering

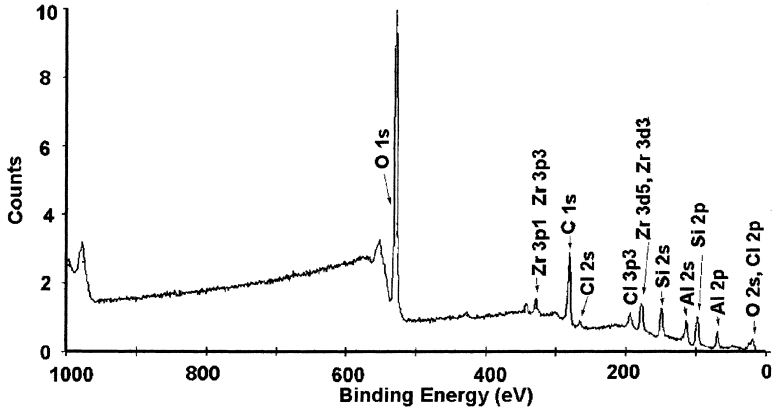

Fig. 4. XPS survey spectrum of $Et(Ind)_2ZrCl_2/MAO/SiO_2$ (preparation 8).

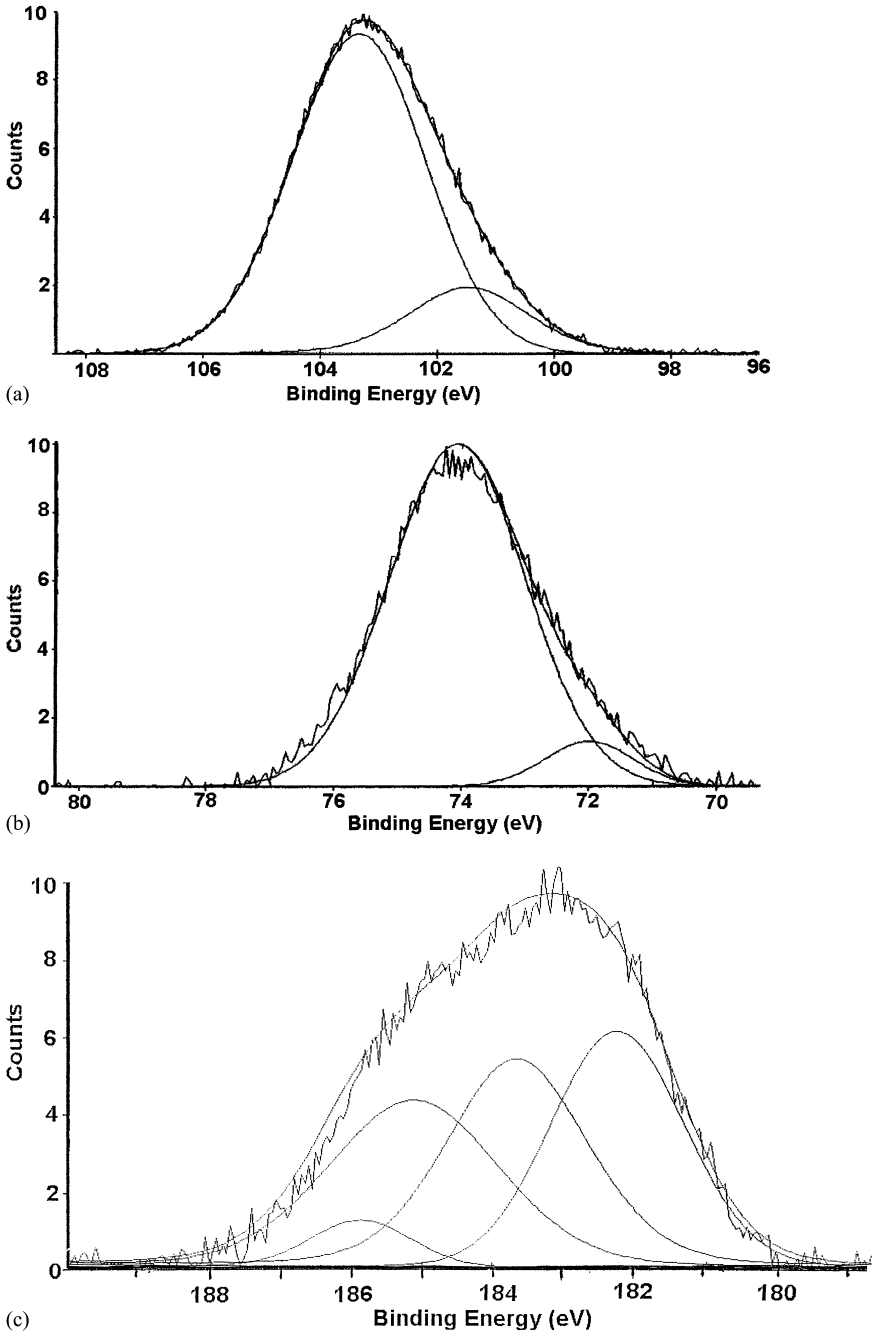

Fig. 5. High resolution XPS of: (a) Si 2p; (b) Al 2p; (c) Zr 3d core level. The small inserted peaks are the curve-fit components, which are summed to obtain the smooth drawn line. The line with a visible noise component is the experimental raw data.

the contribution of both species) is presented in Table 1. The FWHM values for preparations with 6 wt.% Al/SiO_2 are higher than those for 12 wt.% Al/SiO_2, suggesting a higher diversity of zirconium species. This result is in agreement with the hypothesis that for 6 wt.% Al/SiO_2 of initial aluminum concentration, the metallocene anchors on the MAO coating and on the remaining isolated silanol groups.

Leaching of Al in the zirconocene grafting step was also confirmed by XPS analysis. The Al/Si atomic ratio for sample 7 (12.0 wt.% Al/SiO_2) right after MAO impregnation was found to be 1.8; after the metallocene grafting step, it was reduced to 1.4. In other words, after the metallocene grafting step, Al loading was reduced by about 25%.

Based on UV–VIS and XPS analyses, we can propose the existence of two species on silica: dimethylated (**I**) and monomethylated (**II**). Nevertheless, we should not exclude the possibility of direct grafting of zirconocene species by surface reaction with residual OH groups. Moreover, the amount of free TMA present in MAO might also compete for the surface OH groups, generating other alkylaluminum species.

3.2. Catalyst activity

As reported for other supported-metallocene systems [22], the resulting activity is lower than that of the homogeneous catalyst producing copolymer under the same E/P feed ratio (Table 2). This behavior has been attributed to the generation of polymerization inactive species during catalyst grafting and to the steric effect played by the silica support [35].

Table 2
Properties of the resulting copolymers

Preparation	Al/Zr molar ratio	Al_{total}/Zr[a] molar ratio	$M_w \times 10^4$	PDI
6	4	796	3.5	2.1
2	12	760	5.7	2.3
4	16	1138	5.0	2.4
1	21	1143	5.8	2.3
8	24	1369	5.0	2.2
5	28	1710	5.3	2.2
7	38	1721	6.7	2.4
3	66	1985	5.9	2.2
Homo1[b]	–	2000	2.5	1.8
Homo2[c]	–	2000	5.1	2.9
Homo3[d]	–	2000	6.5	2.2

[a] Al present on the support + Al from external MAO.
[b] 60/40 E/P weight ratio in feed.
[c] 70/30 E/P weight ratio in feed.
[d] 80/20 E/P weight ratio in feed.

According to XPS measurements, the resulting catalyst activity for ethylene–propylene copolymerizations can be correlated with the binding energy of Zr 3d electrons in the supported systems. A clear relationship was found, showing that the catalyst activity increases with decreasing Zr $3d^{5/2}$ electron BE of both species (Fig. 6). This is in agreement with

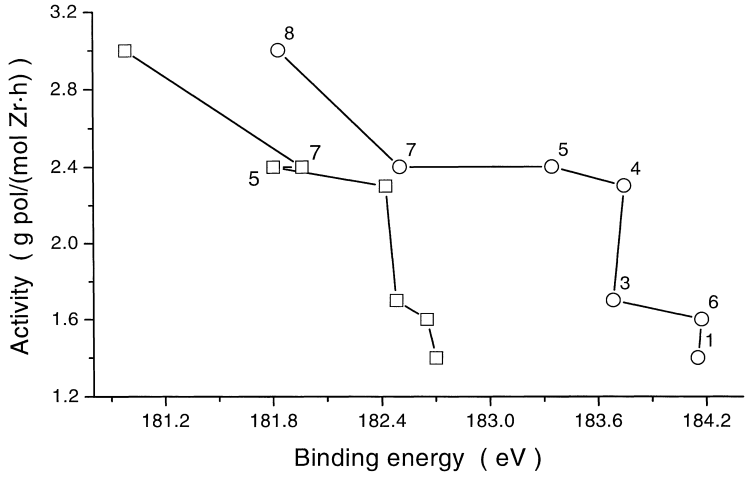

Fig. 6. Relationship between Zr $3d^{3/2}$ binding energy of zirconocene species and catalyst activity in the EP copolymerization: (□) low and (○) high BE Zr species.

previous results from Garbassi et al. [36] reporting Zr 3d binding energies in a series of homogeneous metallocene catalysts with different ligands. The authors correlated this behavior with the activation step, i.e. MAO reaction with the zirconocene to substitute X ligands by methyl groups. Gassmann and Callstrom [37] attributed Zr BEs 181.2 and 180.7 eV, respectively, to $Cp_2ZrClMe$ and Cp_2ZrMe_2 species. Thus, we can probably attribute these two BE signals to the presence of species mono- (high BE) and bimethylated (low BE), in agreement with UV–VIS results.

3.3. Ethylene–propylene copolymers

The produced copolymers were soluble under our polymerization experimental conditions. Therefore, the reaction milieu can be considered homogeneous, while the catalyst system heterogeneous. The gases were continuously fed to the reactor in order to maintain the gas-phase composition constant, and consequently keep a determined concentration of gas mixture in the solvent. The mass transfer effect concerning this polymerization system has been discussed elsewhere [27].

In Fig. 7, the catalyst activity and the ethylene incorporation are directly correlated with the total Al/Zr amount during polymerization. Maximum activity is obtained with incorporation of 88 mol% of ethylene incorporated. At this point, there is a combination between the highest solubility of both monomers in the amorphous growing polymer and the optimum Al/Zr total ratio, which promotes more polymer production. The average molecular weight varied from $(3.5–6.7) \times 10^4\ g\ mol^{-1}$ (see Table 2). The copolymer polydispersity index (PDI) showed no indication of broad molecular weight distribution. PDIs are close to the most probable value proposed by Flory for single-site catalysts [38].

In order to better understand the structure of the obtained polymers and characterization of catalyst systems, one must consider not only average properties but also the distribution of these properties. The chemical composition distribution of the copolymers can also provide information about the nature of the catalyst sites. A direct correlation between crystallinity and chemical composition distribution for polyolefins made with metallocene catalysts has been confirmed through some techniques, like temperature-rising elution fractionation (TREF) and crystallization temperature fractionation (CRYSTAF) [39]. For EP copolymers with high ethylene content, as those obtained in the present work, it is also possible to observe crystallinity. Fig. 8 shows DSC thermograms for some copolymer samples. A shift in the peak of the endothermic curves of polymer fusion can be observed as a function of the Al/Zr ratio during polymerization. High Al/Zr ratios result in higher fusion temperatures, indicating lower

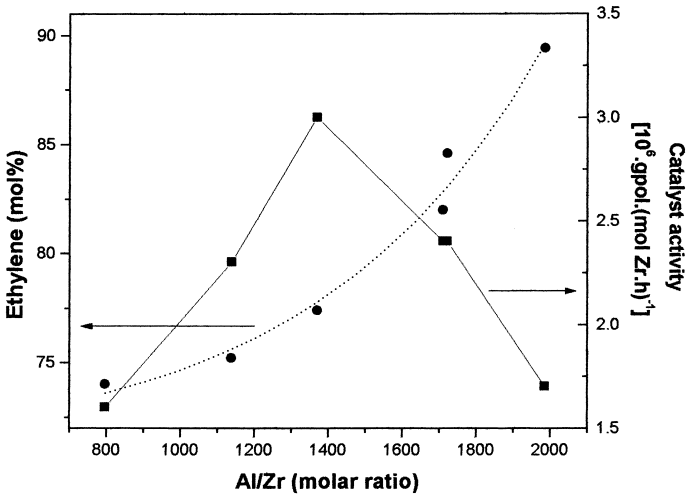

Fig. 7. Catalyst activity and ethylene content as function of the total aluminum amount at the reaction milieu.

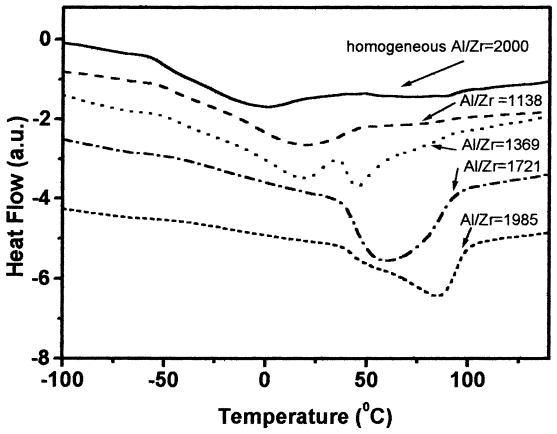

Fig. 8. Endothermic curve of fusion for copolymers produced with different Al/Zr ratios on the support.

propylene incorporation as seen by ^{13}C NMR. Low Al/Zr ratios produce higher comonomer incorporation and a polymer structure similar to that obtained with homogeneous catalyst under Al/Zr = 2000 (60/40 E/P weight ratio in feed).

For intermediate Al/Zr, it is possible to identify two different kinds of crystallites in the same polymer sample, suggesting different chemical compositions regarding the crystalline phase. This heterogeneity in composition can be related to the mass transfer resistance caused by the introduction of the support in the system or to a different nature of the active sites. In the literature, there are studies discussing both aspects using supported-metallocene catalysts. Hoel et al. [18] developed an EP copolymerization model using supported-metallocene systems devoted to explain an unexpectedly broad CCD with these single-site catalysts. Based on experimental and on theoretical results, the authors concluded that the breadth of CCD was a consequence of monomer mass transport limitations during the growth of polymer particles. Recently, Muhle [19], studying the ethylene-1-hexene copolymerization with a supported-metallocene catalyst in a gas-phase process, proposed three different types of active sites on silica. The combined TREF and GPC analysis pointed that the major site was responsible for 76% of the weight polymer fraction, the second for 22%, and the third for 2%. Soga et al. [40] also observed two kinds of poly[ethylene-*co*-(1-hexene)] copolymers with different crystallinity using typical metallocene cocatalyzed by MAO, and attributed to the presence of two kinds of active species.

We also performed CFC analysis of the sample that presented two endothermic peaks in the DSC analysis (Al/Zr = 1369). As seen in Fig. 9, distinct chemical compositions appear with narrow molecular weight distribution. The chemical composition distribution of this sample was also determined by ^{13}C NMR. The low-temperature fraction (under 273 K) was found to consist of 68.8 mol% of ethylene and the high-temperature fraction (up to 273 K) of 80.5 mol%. These results also confirm the heterogeneity of the chemical composition of this sample.

For soluble metallocene catalysts, several authors have observed a correlation between increasing ethylene incorporation and higher molecular weight [41–43]. This tendency can also be observed in Table 3 from the molecular weights and the respective elution temperatures of the cross-fractionated sample. High elution temperatures correspond to the highest molecular weights, which are most crystalline copolymers, richest in ethylene content.

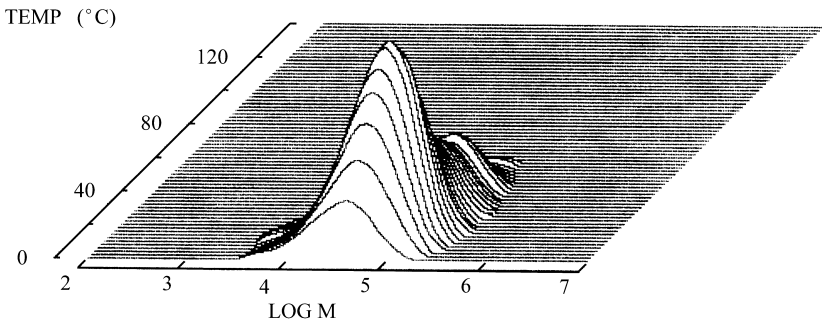

Fig. 9. CFC of EP copolymer produced by preparation 8.

Table 3
Molecular weights from CFC data

Temperature (K)	EP copolymer[a] (wt.%)	$M_n \times 10^{-4}$	$M_w \times 10^{-4}$	PDI
273	59.29	1.87	4.46	2.38
278	3.88	2.80	5.10	1.82
283	6.69	3.44	6.13	1.78
288	7.93	3.64	6.80	1.87
293	6.30	4.13	7.53	1.82
298	4.35	4.62	7.98	1.73
303	3.22	5.32	8.81	1.66
308	2.67	5.03	8.84	1.76
313	1.99	6.24	9.24	1.48
318	1.95	6.55	9.71	1.48
323	0.98	6.26	9.26	1.48
328	0.45	6.02	8.81	1.46
333	0.30	7.75	9.94	1.28

[a] Produced by preparation 8.

These broad CCD might be originated from active species unequally activated by alkylaluminum cocatalyst. The different catalytic species formed during the catalyst preparation can be responsible for these heterogeneous activation. Different alkylated species at the support surface are pointed out in the catalyst section characterization based on UV–VIS and XPS results.

We cannot neglect the possibility that part of the zirconocene grafted on the surface might be leached by the external MAO added in the beginning of the polymerization reaction. However, such homogeneous catalyst systems might lead to an increase in catalyst activity, and the resulting copolymers should present lower M_w in comparison to those produced with supported systems. However, comparing supported catalysts to homogeneous ones under the same experimental conditions (E/P ratio in the feed, and roughly equal Al/Zr ratio, i.e. compare $Al/Zr = 2000$ for homogeneous to $Al/Zr = 1985$; preparation 3, in Table 2) showed different catalyst activities and resulting copolymer properties. Under such conditions, the non-supported catalyst exhibited catalyst activity of 11×10^6 g polymer $(\text{mol Zr h})^{-1}$, that is, 10 times higher than that observed in the case of catalyst 3 (1.7×10^6 g polymer $(\text{mol Zr h})^{-1}$). The reduction in activity for the supported system is usually attributed to the generation of surface inactive species, besides steric effect played by the silica surface itself. Copolymers produced by supported-catalyst systems showed higher M_w than those obtained with homogeneous systems. This fact could be attributed to the blocking of one of the sides of the active site by the support, hindering the deactivation step. In other words, the β-elimination transfer between two metallocene centers is hindered, resulting in a larger growth of the polymer chain, and so in a higher molecular weight. Besides, propylene incorporation in the resulting EP copolymers was 10.6 and 33.2 for the supported and homogeneous catalysts, respectively. Such results suggest once again a steric effect played by the support surface. These observations suggest that leaching of active surface species by external MAO is irrelevant under our experimental conditions.

The overall microstructure of the produced copolymers can be evaluated by the concentration of triads (Fig. 10). For comparative reasons, data from the homogeneous system were also included. The characteristics of the polymers produced in homogeneous system under different feed conditions can be observed in Table 2, and their concentration of triads was used to construct the trend lines observed in Fig. 10. The average microstructure of the copolymers produced with the supported system follows the same trend in propylene incorporation as the homogeneous, indicating that the catalyst in the support produces a random copolymer like the homogeneous one.

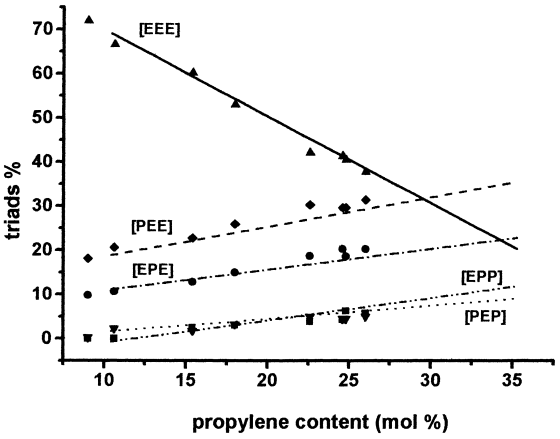

Fig. 10. Copolymer microstructure for samples produced with different Al/Zr ratios on the support (trend lines drawn with data from homogeneous copolymerizations).

4. Conclusions

Through the use of experimental design, it was possible to observe that only the initial Al and Zr solution concentrations are significant for the Zr loading on the support. The final Al loading on the support is only determined by the availability of isolated silanol groups, which for our silica pretreatment conditions is approximately between 6 and 8 wt.% Al/SiO_2.

The UV–VIS analysis permitted us to observe that during the catalyst preparation step, mono- and dialkylated species are formed by the interaction of MAO desorbed from the support and the remaining catalyst precursor. Leaching in the preparative step was also confirmed by XPS analysis.

At the 95% confidence level, we cannot observe any direct relationship between the preparative variables and catalyst activity, nor copolymer properties. However, it was observed that the increase in the catalyst activity for ethylene–propylene copolymerizations seems to be correlated to the decrease of Zr $3d^{5/2}$ electron binding energy of the supported-zirconocene species.

According to our results, it is possible to control the average ethylene incorporation in the copolymers by changing the Al/Zr ratio. The molecular weight distribution of the copolymers is narrow, but according to DSC and CFC data, there is a broad chemical composition depending on the Al/Zr ratio used.

Concerning the copolymer microstructure produced by the supported system follows the same trend as those obtained by the homogeneous ones with the propylene incorporation, indicating that the catalyst in the support produces a random copolymer.

Acknowledgements

Thanks are due to Ms. Paula P. Greco for helping during catalyst preparation. This work has been supported by Brazilian agencies CNPq and FINEP. M.C. Haag has a CNPq fellowship. Financial support for Prof. J.H.Z. dos Santos has been provided by the Japan Society for Promotion of Science (JSPS).

References

[1] J. Scheirs, W. Kaminsky (Eds.), Metallocene-Based Polyolefins, Vol. 1, Wiley, West Sussex, 2000.
[2] H.G. Alt, A. Köppl, Chem. Rev. 100 (2000) 1205.
[3] C. Janiak, in: A. Togni, R.L. Halterman (Eds.), Metallocenes: Synthesis Reactivity Applications, Vol. 2, Part A, Wiley/VCH, Weinheim, 1998, p. 547.
[4] M.C. Haag, J.H.Z. dos Santos, F.C. Stedile, J. Dupont, J. Appl. Polym. Sci. 74 (1999) 1997.
[5] G.G. Hlatky, Chem. Rev. 100 (2000) 1347.
[6] H.T. Ban, T. Arai, C.-H. Ahn, T. Uozumi, K. Soga, Curr. Trends Polym. Sci. 4 (1999) 47.
[7] M.R. Ribeiro, A. Deffieux, M.F. Portela, Ind. Eng. Chem. Res. 36 (1997) 1224.
[8] M. Balsam, P. Barghoorn, U. Stebani, Die Angew. Makromol. Chem. 267 (1999) 1.
[9] P. Pietikinen, J.V. Seppälä, Macromolecules 27 (1994) 1325.
[10] A. Zambelli, A. Grassi, Makromol. Chem., Rapid Commun. 12 (1991) 523.
[11] C. Lehtinen, B. Löfgren, Eur. Polym. 33 (1997) 115.
[12] J.W. Chien, D. He, J. Polym. Sci.: Polym. Chem. 29 (1991) 1585.
[13] M. Galimberti, M. Destro, O. Fusco, F. Piemontesi, I. Camurati, Macromolecules 32 (1999) 258.
[14] R. Krasvchenko, R. Waymouth, Macromolecules 31 (1998) 1.
[15] M. Galiberti, F. Piemontese, O. Fusco, I. Camurati, M. Destro, Macromolecules 31 (1998) 3409.
[16] M. Galimberti, N. Mascellani, F. Piemontesi, I. Camurati, Macromol. Rapid Commun. 20 (1999) 214.
[17] J.W. Chien, D. He, J. Polym. Sci.: Polym. Chem. 29 (1991) 1603.
[18] E.L. Hoel, C. Cozewith, G.D. Byrne, AIChE J. 40 (1994) 1669.
[19] M.E. Muhle, in: Proceedings of the MetCon'98, Houston, June 1998.
[20] J.B.P. Soares, Polym. React. Eng. 6 (1998) 225.
[21] J.H.Z. dos Santos, M.B. da Rosa, C. Krug, F.C. Stedile, M.C. Haag, J. Dupont, M.C. Forte, J. Polym. Sci.: Part A: Polym. Chem. 37 (1999) 1987.
[22] C. Krug, M.B. da Rosa, J.H.Z. dos Santos, J. Dupont, F.C. Stedile, I.J.R. Baumvol, in: Proceeding of the XVI Simposio Ibero-Americano de Catalisis, Cartagena de Índias, 23–28 August 1998, p. 2009.
[23] G.E.P. Box, G.W. Hunter, J.S. Hunter, Statistics for Experimenters, Wiley, New York, 1978.
[24] J.H.Z. dos Santos, S. Dorneles, F.C. Stedile, J. Dupont, M.C. Forte, I.J.R. Baumvol, Macromol. Chem. Phys. 198 (1997) 3529.
[25] D. Coevoet, H. Cramail, A. Deffieux, Macromol. Chem. Phys. 199 (1998) 1451.
[26] J.H.Z. dos Santos, H.T. Ban, T. Teranishi, T. Uozumi, T. Sano, K. Soga, J. Mol. Catal. A: Chem. 158 (2000) 541.
[27] M.C. Haag, J.H.Z. dos Santos, J. Dupont, A.R. Secchi, J. Appl. Polym. Sci. 70 (1998) 1173.
[28] M.C. Haag, J.H.Z. dos Santos, J. Dupont, A.R. Secchi, J. Appl. Polym. Sci. 76 (2000) 425.
[29] L.P. Linderman, N.O. Adams, Anal. Chem. 43 (1975) 795.

[30] J.H.Z. dos Santos, A. Larentis, M. Da Rosa, C. Krug, F.C. Stedile, J. Dupont, M.C. Forte, Macromol. Chem. Phys. 200 (1999) 3529.
[31] E.F. Vansant, P. Van der Voort, K.C. Vracken, Stud. Surf. Sci. Catal. 93 (1995) 59.
[32] P.J.J. Pieters, J.A.M. van Deek, M.F.H. van Tol, Makromol. Rapid Commun. 16 (1995) 463.
[33] J. Pédeutour, D. Coevoet, H. Cramail, A. Deffieux, Macromol. Chem. Phys. 200 (1999) 1215.
[34] T.L. Barr, Modern ESCA. The Principles and Practice of X-Ray Photoelectron Spectroscopy, CRC Press, Boca Raton, 1994.
[35] W. Kaminsky, J. Chem. Soc., Dalton Trans. (1998) 1413.
[36] F. Garbassi, L. Gila, A. Proto, J. Mol. Catal. A: Chem. 101 (1995) 199.
[37] P.G. Gassmann, M.R. Callstrom, J. Am. Chem. Soc. 109 (1987) 7875.
[38] P.J. Flory, Principles of Polymer Chemistry, Cornell University Press, Ithaca, 1953.
[39] B. Monrabal, J. Blanco, J. Neto, J.B.P. Soares, J. Polym. Sci.: Part A: Polym. Chem. 37 (1999) 1099.
[40] K. Soga, T. Uozumi, T. Arai, S. Nakamura, Macromol. Rapid Commun. 16 (1995) 379.
[41] K. Soga, T. Arai, H. Nozawa, T. Uozomi, Macromol. Symp. 97 (1995) 53.
[42] N. Naga, Y. Ohbayashi, K. Mizunama, Macromol. Rapid Commun. 18 (1997) 837.
[43] D. Lee, K. Yoon, J. Park, B. Lee, Eur. Polym. J. 53 (1997) 447.